Atmospheric Environment 45 (2011) 3447–3453

Contents lists available at ScienceDirect

Atmospheric Environment

journal homepage: www.elsevier.com/locate/atmosenv

Mixing state of biomass burning particles by single particle aerosol mass spectrometer in the urban area of PRD, China

Xinhui Bi [a,*], Guohua Zhang [a,b], Lei Li [c], Xinming Wang [a], Mei Li [c], Guoying Sheng [a], Jiamo Fu [a,c], Zhen Zhou [c]

[a] State Key Laboratory of Organic Geochemistry, Guangdong Province Key Laboratory of Utilization and Protection of Environmental Resource, Guangzhou Institute of Geochemistry, Chinese Academy of Sciences, Guangzhou 510640, PR China
[b] Graduate University of Chinese Academy of Sciences, Beijing 100039, PR China
[c] School of Environmental and Chemical Engineering, Shanghai University, Shanghai 200444, PR China

ARTICLE INFO

Article history:
Received 13 December 2010
Received in revised form
11 March 2011
Accepted 11 March 2011

Keywords:
Biomass burning
Mixing state
Single particle
Nitrate
Sulfate
SPAMS
ATOFMS
Aerosol
PRD

ABSTRACT

Single particle aerosol mass spectrometer (SPAMS) was used to characterize the single particle size and chemical composition of submicron aerosols in the urban area of the Pearl River Delta region, China, for the period April 30 through May 22, 2010. A total of 696,465 particles were sized and chemically analyzed with both positive and negative ion spectra, in which 141,338 biomass burning particles were identified representing a significant source of submicron particles ~20.3% by number. The results have revealed that biomass burning particles have experienced extensive atmospheric processing, finding that as much as 90.5% of the particles have internally mixed with secondary inorganic species. Biomass burning particles were clustered into six distinct particle groups, comprising of K–Ca-rich, K–Na-rich, K–organic carbon (K–OC), K–elemental carbon (K–EC), K–the mixture of OC and EC (K–OCEC) and K–Secondary. K–OC was the largest contributor with a fraction of 22.9%, followed by K–Secondary type (21.4%) and K–OCEC (19.0%). K–Na-rich type was observed in 11.9% of the particles and 90% internally mixed with EC. The fraction of nitrate in biomass burning particles was 10% higher than in the non-biomass burning particles. The sodium and potassium in biomass burning particles could exhibit high affinity for nitrate gases during neutralization reactions, facilitating the particulate nitrate formation. Meanwhile, the particulate sulfate in particles in the droplet-mode size was also enhanced. The results added appreciably to the knowledge of aerosol characteristics in the PRD region atmosphere and could be applied to the climate models.

1. Introduction

Biomass burning is a significant source of anthropogenic aerosol particles (Andreae and Merlet, 2001) and represents the largest source of submicron particles: approximately 33–39% by number from 1 to 7 km of the troposphere (Pratt and Prather, 2010). Biomass burning activities emit large amounts of carbonaceous aerosol containing black carbon and organic constituents such as polycyclic aromatic hydrocarbons (PAHs) which have potential carcinogenic, mutagenic and genotoxic effects on humans. Up to 38% of the total emissions of black carbon in China have been attributed to biomass burning (Streets et al., 2001). Moreover, biomass burning particles can effectively scatter and absorb solar radiation, and are good cloud condensation nuclei (Reid et al., 2005a, 2005b). Therefore, biomass burning has always been of interest to scientists. In addition, biomass burning aerosols would undergo aging processes as they travel through the air, causing significant changes to their physiochemical and optical properties (Reid et al., 2005a) that merits consideration in climate models.

Single particle mass spectrometer, such as aerosol time-of-flight mass spectrometer (ATOFMS), has been extensively used to measure the aerodynamic size and chemical composition of individual aerosol particles (Gard et al., 1997, 1998; Guazzotti et al., 2001; Liu et al., 2003; Toner et al., 2006; Shields et al., 2008; Spencer et al., 2008; Pratt and Prather, 2009). It has been proved to be a powerful tool for analyzing the mixing state and formation mechanisms of aerosols in single particle levels (Gaston et al., 2010; Angelino et al., 2001; Moffet et al., 2004; Freney et al., 2006; Denkenberger et al., 2007; Moffet and Prather, 2009; Wang et al.,

* Corresponding author. Tel.: +86 20 85290195; fax: +86 20 85290288.
E-mail address: bixh@gig.ac.cn (X. Bi).

1352-2310/$ – see front matter © 2011 Elsevier Ltd. All rights reserved.
doi:10.1016/j.atmosenv.2011.03.034

2009a; Yang et al., 2009). These accomplishments are extremely helpful to understand the impact of aerosols on the global climate.

The Pearl River Delta (PRD) region, located at the center of Guangdong Province, China, is an area of 41,700 square kilometers, with a population of 43 million people. Rapid urbanization and industrialization in the last few decades have caused substantial atmospheric pollution. The Program of Regional Integrated Experiments of Air Quality over Pearl River Delta (PRIDE-PRD) was conducted in 2004 and 2006 to observe the chemical and physical processes controlling the key parameters of aerosol, including chemical composition, size distribution, and optical properties in the PRD region (Cheng et al., 2008; Hua et al., 2008; Zhang et al., 2008; Sugimoto et al., 2009; Xiao et al., 2009). The previous studies utilizing conventional filter aerosol sampling techniques showed that biomass burning had a strong impact on the air quality of the PRD region (Hagler et al., 2006; Wang et al., 2007; Bi et al., 2008). The chemical composition of biomass burning particles was measured using off-line analysis (Wang et al., 2009b), which required long collection periods in which additional chemical reactions on the filters may have biased the data. To the best of our knowledge, there has heretofore been scant use of single particle mass spectrometry to analyze the mixing state of biomass burning and its impact on particle chemistry in China (Li and Shao, 2009; Li et al., 2010).

An experiment was designed to study size-resolved characteristics of submicron aerosols in urban PRD using a single particle aerosol mass spectrometer (SPAMS) with a focus to study the chemical composition, size and mixing state of biomass burning particles. The data acquired could be utilized to assess the influence of biomass burning on the region's air quality and climate.

2. Experimental section

2.1. Sampling

Single particle measurement was carried out in 2010 between April 30 and May 22, with occasional maintenance and recalibration stand-downs, using an SPAMS made by Hexin Analytical Instrument Co., Ltd (Li et al., 2011). The hourly variation of temperature, humidity, visibility and wind directions are presented in Figure S1 of the Supplementary Material. The temperature varied between 19 and 33 °C, with an average of 26.0 °C, with relative humidity varying more widely between 22 and 100%. The sample air was introduced from the platform about 10 m above ground in a three-story building at the Guangzhou Institute of Geochemistry, situated approximately 100 m from the major traffic artery and 2 km from the city center. The air was sampled through an 8 mm copper tube connected to the SPAMS instrument, which was installed in an air-conditioned room located on the first floor of the building. Because of the relative long tubing (approx. 10 m) and low sampling flow rate, an additional pump (operated at a flow rate of 5 L min^{-1}) was used to shorten the residence time of the air in the tube. A $PM_{2.5}$ cyclone was installed upstream the sample inlet to exclude coarse particles. No specific tests were run to check for leaks or contamination from the use of a copper-based inlet, as such tainting problems have not been typically observed in previously published papers.

2.2. Single particle mass spectrometry

Particles detection method of SPAMS has been described elsewhere (Li et al., 2011). Briefly, aerosol particles are introduced into vacuum pumped SPAMS through a 0.1 mm critical orifice at a flow of 80 mL min^{-1} due to the pressure drop from ~760 to ~2.2 Torr. They are then focused and accelerated to specific velocities characteristic of their vacuum aerodynamic diameters while passing through the aerodynamic lens, followed by the sizing region, where velocities of individual particles are determined by two continuous diode Nd:YAG laser beams operated at 532 nm and located 6 cm apart. Desorption/ionization is applied subsequently by a 266 nm Nd:YAG laser that is triggered exactly based on the velocity of the specific particle as measured in the sizing chamber. The positive and negative fragments are detected by a dual-polarity time-of-flight mass spectrometer. In this study, the energy of desorption/ionization laser was regulated at about 0.6 mJ. The power density of the desorption/ionization laser was kept relatively low, at about 1.06E+08 W cm^{-2}. Polystyrene latex spheres (Nanosphere Size Standards, Duke Scientific Corp., Palo Alto) of 0.2–2 μm in diameter were used to calibrate the sizes of the detected particles.

2.3. Analysis of single particle data

Particles sizes and mass spectra information were used to create peak lists, using TSI MS-Analyze software. The peak lists were then imported into MatLab 7.1 (The Mathworks Inc.). Peak thresholds were set to record only those peaks with heights greater than 10 units and area greater than 20 units to distinguish peaks from the background noise in the mass spectra. The YAADA 2.1 toolkit (www.yaada.org) was utilized to search and analyze the imported information for individual particles. Because the particle-detection efficiency of the SPAMS exhibits strong dependent on particle size (Allen et al., 2000; Su et al., 2004), each size range represents the relative counts of different particle types and not the actual atmospheric concentration, but the size distributions remain useful for comparing particle types.

3. Results and discussion

The single particle results presented in this work cover aerodynamic diameters between 0.2 and 1.2 μm. A total of 696,465 single particle mass spectra were collected over the course of the campaign. Biomass burning particles were queried by searching for given *m/z* ratios, which is given in Table 1, based on previous lab studies (Silva et al., 1999; Yang, 2010). A total of 141,338 biomass burning particle mass spectra were obtained, which contributed approximately 20.3% on average to the total submicron particles count.

3.1. Chemical composition

The average digitized mass spectrum of biomass burning particles is displayed in Fig. 1. The dominant peaks in the positive ion mass spectra were potassium (K^+), sodium (Na^+), organics and carbon cluster ions. Sulfate, nitrate, CN^- and carbon cluster ions were the most common peaks observed in the negative ion spectra. The other species included metallic elements such as copper (Cu^+), vanadium (V^+) and lead (Pb^+). As much as 90.5% of the biomass

Table 1
The SPAMS markers used to search for biomass burning particles in this study.

Species	*m/z*	Marker ion	Area	Relative area	Function
K and K-clusters	39 ± 0.5	$[K]^+$	500	0.05	and
	113 ± 0.5, 115 ± 0.5	$[K_2Cl]^+$	50	0.005	or
	213 ± 0.5, 215 ± 0.5	$[K_3SO_4]^+$	50	0.005	or
Levoglucosan	−45 ± 0.5	$[CHO_2]^-$	50	0.005	or
	−59 ± 0.5	$[C_2H_3O_2]^-$	50	0.005	or
	−73 ± 0.5	$[C_3H_5O_2]^-$	50	0.005	or
CN	−26 ± 0.5	$[CN]^-$	50	0.005	or

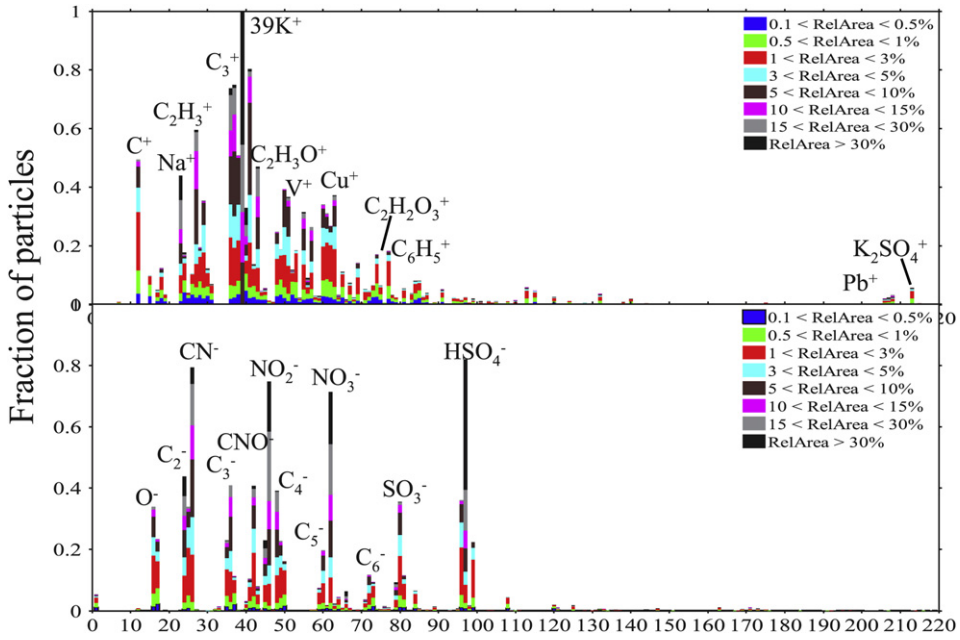

Fig. 1. Average digitized positive (top panel) and negative (bottom panel) ion mass spectrum of biomass burning particles.

burning particles were found to internally mix with secondary inorganic species, more or less in amount, suggesting that these particles had undergone significant secondary processing during transport.

A neural network algorithm, ART-2a, grouped the data into clusters of particles with similar mass spectral features over 20 iterations, with a vigilance factor of 0.7 and a learning rate of 0.05. The grouping yielded 578 clusters, with the top 200 clusters representing over 91% of the mass spectra from the study. Further manual classification was used to reduce the number of main classes to six. The remaining 9% of clusters characterized by low-mass spectral resolution was grouped into one class referred to as "Unclassified". Ca and Na, which are often regarded as originating from dust and sea salt, respectively (Pastor et al., 2003; Dall'Osto and Harrison, 2006; Yang et al., 2009), were not removed because these elements were also detected in the smoke of biomass burning (Silva et al., 1999; Yamasoe et al., 2000; Schmidl et al., 2008). Both Ca–EC and Na–EC particles have been observed in vehicle exhausts (Sodeman et al., 2005; Toner et al., 2006). Therefore, the Ca-rich and Na-rich biomass burning particles might be resulted from the mixing of biomass burning and vehicular emissions. This choice of markers allows the selection of all particles present in biomass burning.

An area matrix for each of the top six particle types is given in Fig. 2, and a brief description of each type follows. 39$[K]^+$, which is considered to be a good marker for biomass burning (Andreae, 1983), was present in all of the types. K–Ca-rich was characterized by ion peaks in the positive ion spectra for 40$[Ca]^+$, 39$[K]^+$, 23 $[Na]^+$, a smaller 56$[CaO]^+$; and by peaks in the negative spectra for $-26[CN]^-$, carbon cluster ions $-12[C]^-$, $-24[C_2]^-$…$[C_n]^-$. K–Na-rich contained intense ions at 23$[Na]^+$, 39$[K]^+$ and dual polarity carbon cluster ions 12$[C]^{\pm}$, 24$[C_2]^{\pm}$…$[C_n]^{\pm}$. K–OC particles were identified by 39$[K]^+$ and OC marker ions such as 15$[CH_3]^+$, 27 $[C_2H_3]^+$, 29$[C_2H_5]^+$ and 43$[C_2H_3O]^+$ (Spencer and Prather, 2006). K–EC particles contained 39$[K]^+$ and dual polarity carbon cluster ions (12$[C^{\pm}]$, 24$[C_2]^{\pm}$, 36$[C_3]^{\pm}$,…, $[C_n]^{\pm}$) and without OC marker ions or with really low intensity of OC marker ions. K–OCEC exhibited a signature indicative of internally mixed with OC marker ions and EC cluster ions as well as a strong peak 39$[K]^+$. The K-Secondary particles were characterized by intense 39$[K]^+$ without or very low other ions in the positive spectra as well as strong sulfate at m/z $-97[HSO_4]^-$ and nitrate at m/z $-46[NO_2]^-$ and -62 $[NO_3]^-$ in the negative spectra. Sulfate and nitrate are generally regarded as secondary species although they can be emitted from the primary sources.

Fig. 3 showed that K–OC was the most abundant among the seven clusters with a fraction of 22.9%, followed by K–Secondary (21.4%) and K–OCEC (19.0%). The K–Ca-rich type was the least one accounting for 5% of the analyzed particles. It is important to note that K–Na-rich type was observed in 11.9% of the particles. The color stacks of the carbon cluster ions peak demonstrate that approximately 90% of the K–Na-rich particles internally mixed with EC (Figure S3), which differs from the sea salt particles (Dall'Osto et al., 2004; Dall'Osto and Harrison, 2006; Spencer et al., 2008). Pearson correlation analysis indicated that the unscaled SPAMS counts in 1 h resolution of certain particle types have a correlative relationship, particularly between K–EC and K–Na-rich (correlation coefficients $r = 0.894$, $p < 0.01$) (Table S1). The good correlation between particle types suggests common or similar sources, and/or that they were subject to similar processes.

The temporal profile (1 h resolution) of the six particle types between May/14/10 and May/21/10 is shown in Figure S3. These figures show that each type exhibited a similar pattern, and did not show strong diurnal trends although generally there was a peak in the night. The peaks occurred in the night were due to the portioning of semi-volatile compounds from the vapor phase into the particle phase and/or the formation of a stable nocturnal inversion layer. Peaks occurred in the early morning hours or in the afternoon were most likely correlated with particular sources and events. The particle types excluding K-Secondary showed correlations with relative humidity and anti-correlations with temperature.

For a more detailed examination, Fig. 4 illustrates the percentage of the particle types as a function of their aerodynamic diameters (in 50 nm bins). Although nearly all of the particle types were observed in all size ranges, the size distribution of the biomass burning particles was bimodal with significant condensation and droplet-mode fractions. K–EC and K–Na-rich were the major

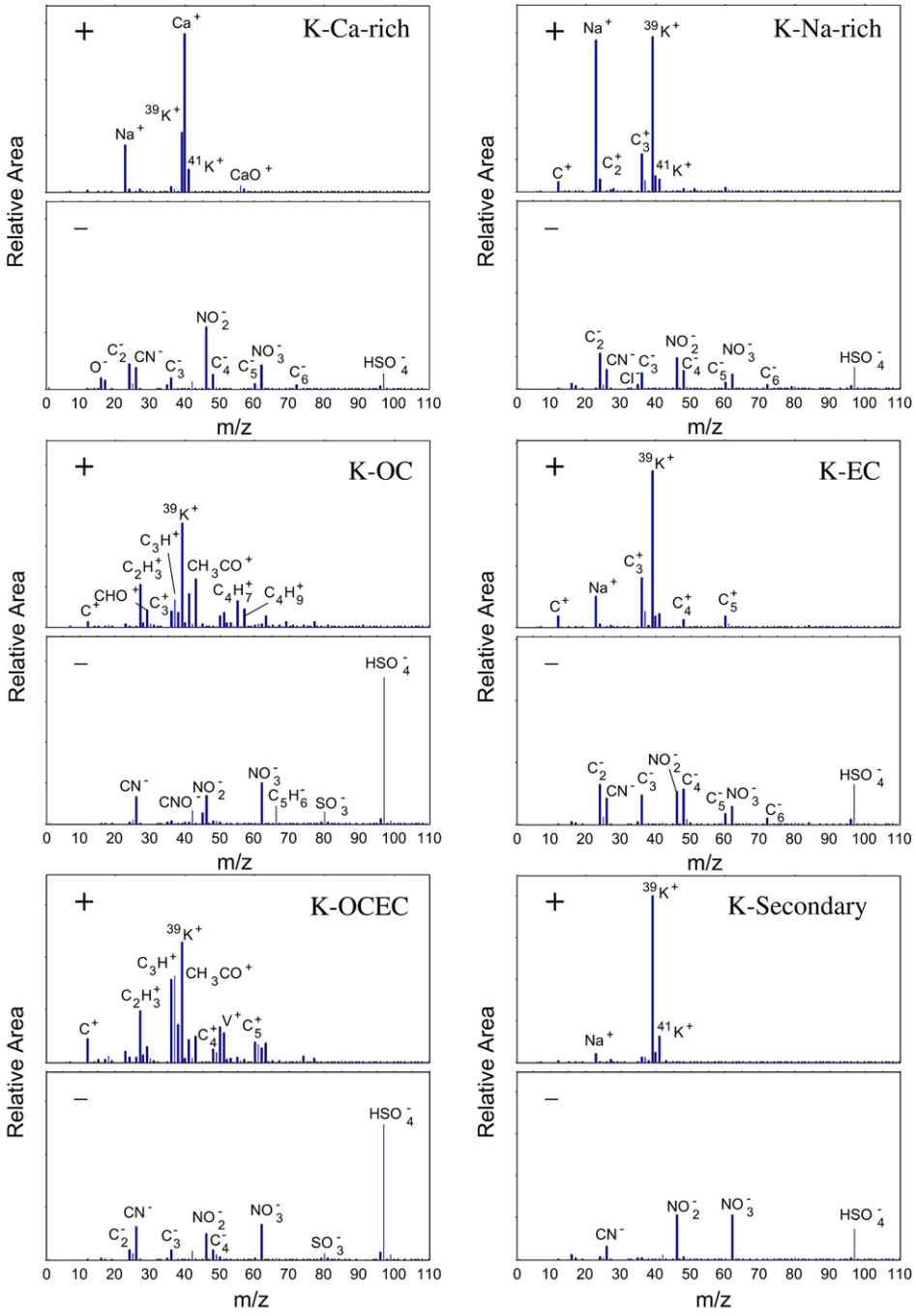

Fig. 2. Area matrices for the top six particle classes (K–Ca-rich, K–Na-rich, K–OC, K–EC, K–OCEC, K-Secondary) observed in urban area of the PRD region.

components, accounting for 65.8% of the condensation particles ranging from 200 to 400 nm (d_{va}); as the particle size increasing, their contribution decreased. From 500 to 1200 nm, the chemical composition became relatively constant with K–OC being the dominant type, suggesting that the organic aerosol component was largely from secondary formation rather than primary emission. K–EC particles aged with and without extra OC coating accounted for 18.1% and 6.6% of particles greater than 500 nm in diameter, respectively. The K–EC particles in droplet-mode support that addition of sulfate through in-cloud processing, and nitrate through heterogenic reactions, caused the transition from the condensation mode (Yu et al., 2010).

3.2. Mixing state of biomass burning particles with secondary species

The mixing state of the original particles would alter the light absorption and surface properties of particles. Studies have showed that internally mixed EC–sulfate and OC-coated EC particles enhanced atmospheric absorption ability by increasing a particle's absorption efficiency by about 3 times compared to uncoated EC (Jacobson, 2001; Bond et al., 2006), and their ability as CCN by hydrophobic to hydrophilic surface alteration (Rose et al., 2010). Presented here are the first in situ chemically resolved measurements of the mixing state of biomass burning particles in the PRD

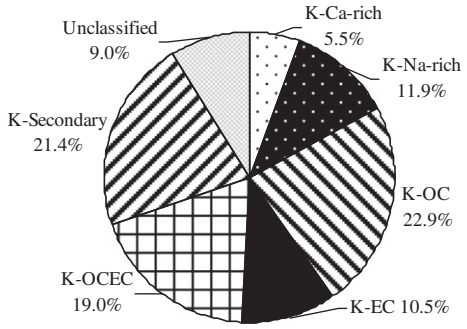

Fig. 3. Relative number abundance distribution of the seven main classes of biomass burning particles obtained using ART-2a (the remaining 9% of cluster was referred to as "Unclassified")

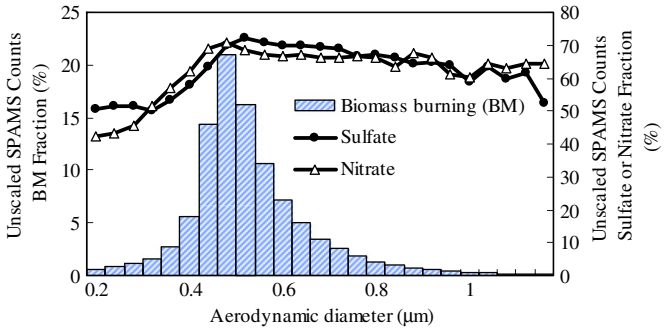

Fig. 5. Number fraction of biomass burning particles mixed with secondary species as a function of aerodynamic diameter.

region. This study shows that 67.1% and 66.8% of biomass burning particles were found to internally mix with sulfate and nitrate, respectively. The identification of sulfate and nitrate was based on the criterion that the relative areas of the peaks were more than 0.05 for sulfate and nitrate. Sulfate-only particles were present in ~23.7% of the total biomass burning particles, and had stronger correlations with K–OC and K–OCEC than with the other types. In contrast, nitrate-only particles accounted for 23.4% of the particles, and were more internally mixed with K–Ca–, K–Na–, and K–Secondary particles. These results suggest different formation pathways for sulfate and nitrate. Particle-phase sulfate resulted predominantly from sulfur dioxide oxidation in the cloud free atmosphere (Tyndall and Ravishankara, 1991) and, more commonly, SO_2 conversion in clouds and fogs (Gurciullo and Pandis, 1997; Zhang et al., 1999). The preferential enrichment of nitrate in inorganic ions-rich particles was evidence of a predominant gas-phase source for nitric acid and precursors, followed by partitioning and heterogeneous/aqueous chemistry. Sulfate and nitrate mixture (accounting for >43.4% of the total biomass burning particles) coexisted in the K–OC, K–OCEC and K-Secondary types.

The percentage of biomass burning particles mixed with sulfate and nitrate is presented as a function of aerodynamic diameter in Fig. 5. The fraction with sulfate and nitrate increased with particle size, ranging from 49.9% to 72.0% and 42.2% to 70.8%, respectively, which is different from the non-biomass burning particles, which was referred to as the particles excluding the biomass burning-containing particles from the total particles detected by SPAMS. The fraction of the non-biomass burning particles mixed with sulfate was about 75% in the condensation mode particles, and decreased with increased particle size ranging between 72% and 46% in the droplet-mode particles. However, the fraction with nitrate increased with particle size ranging between 14% and 73% within the submicron size range. Compared with the non-biomass burning particles (Figure S4), it can be seen that the particulate sulfate formation in biomass burning particles decreased in the condensation mode, and increased in the droplet mode. Nitrate formation increased, and the changes occurred mainly with the condensation mode particles. Nitrate-containing particles formed mainly through the gas-phase reactions of NO_2 with OH radicals, followed by HNO_3 transformation from gas phase into particles via neutralization reactions and heterogeneous oxidation of nitrogen oxide on the particle surface (Hu et al., 2008; Wang et al., 2009a). The preferential formation of nitrate in biomass burning particles was attributed to the reaction of its gaseous precursors with particles. Alkalinic particle types such as K^+ and Na^+-rich would be expected to have a high affinity for acidic gases during aqueous processing. This processing by acids likely neutralized much of the alkaline particles, driving gaseous nitric acid to partition to the particles (Lee et al., 2003; Wang et al., 2009a). Potassium was the most abundant ion in the biomass burning particles. The K–Na-rich particles accounted for 11.9% of the total biomass burning particles, but accounted up to 35.6% of the condensation mode particles. The high percentage of Na in the small particles may facilitate the reaction of gaseous HNO_3 with particles. Xiao et al. (2009) studied the formation of submicron sulfate aerosol

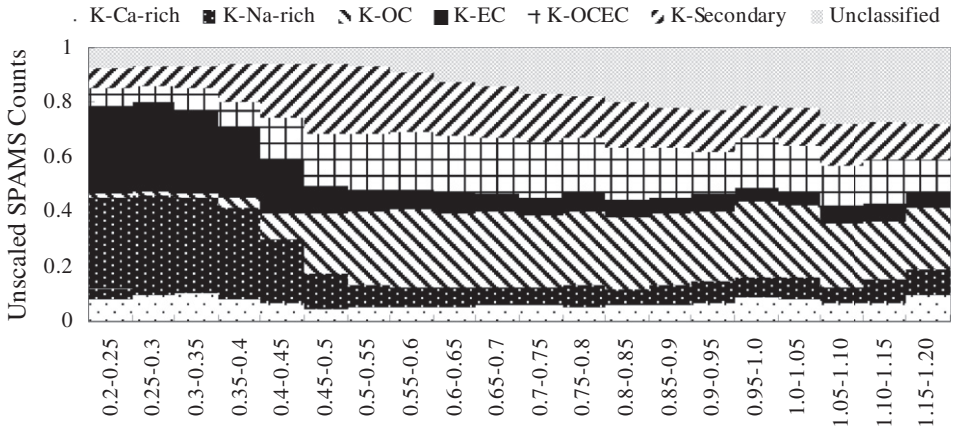

Fig. 4. Chemical composition as a function of aerodynamic diameter, plotted in 0.05 μm resolution.

in the urban area of the PRD region, and observed the rapid increased of sulfate in the condensation mode due to gas-phase oxidation of SO_2 by OH radical. By a similar formation mechanism, sulfate and nitrate competed, with the enhanced nitrate blocking the formation of sulfate in the condensation mode particles. The enhanced sulfate formation in the droplet-mode particles was possibly due to rich ions produced by biomass burning, which made a stronger hydrophilic surface, thus favored the sulfate formation by in-cloud process. Therefore, both the potassium and sodium biomass burning particles could have their roles in the internal mixing of sulfate and nitrate in the PRD region, which was also observed with clean airflow (Murphy and Thomson, 1997).

Previous studies have also shown that biomass burning significantly contributed to the regional haze, and led to deterioration of air quality (bin Abas et al., 2004; Li and Shao, 2009; Warneke et al., 2009; Li et al., 2010). The light-scattering efficiency of fine particulate nitrate was also reported to be higher than that of sulfate (Appel et al., 1985). This study shows that biomass burning causes air quality deterioration not only by the emission of gas and particles, but also by the facilitating formation of nitrate particles during the transport.

4. Conclusions

To reduce the assumptions and uncertainties associated with modeling the impacts of biomass burning aerosols on direct and indirect radiative forcing, direct measurements of the chemistry of atmospheric particles are required. SPAMS analysis of biomass burning particles in this study shows that approximately 90.5% of biomass burning particles were internally mixed with inorganic secondary species, suggesting they underwent significant processing during transport to the sampling site. Three particle types – K–OC, K–OCEC and K–Secondary – dominated the submicron aerosols. K–EC and K–Na-rich were more prevalent with the condensation mode particles, while K–OC and K–OCEC were abundant with the droplet-mode particles. Sulfate was preferentially mixed with the organics-containing particles, while nitrate tended to mix with the inorganic ions-rich particle type. The abundance of inorganic ions in the biomass burning particles maybe facilitate the formation of particulate nitrate in the condensation mode and of particulate sulfate in the droplet mode. Further research will focus on the effects of meteorological conditions on the mixing state of biomass burning particles in PRD and the impact of biomass burning on particle chemistry during haze.

Acknowledgments

The authors would like to thank the National Nature Science Foundation of China (No. 41073077), the Knowledge Innovation Key Projects of the Chinese Academy of Sciences (kzcx2-yw-139), the Science and Technology Project of Guangdong Province (No. 2010A060803007), and Guangzhou Institute of Geochemistry, Chinese Academy of Sciences (GIGRC-09-02) for providing the finical support to carry out this research. The authors gratefully acknowledge Dr. Zhengxu Huang for his assistance in the maintenance of the SPAMS equipment. This is contribution No. from GIGCAS1302.

Appendix. Supplementary material

Supplementary information associated with this article can be found in the online version, at doi:10.1016/j.atmosenv.2011.03.034.

References

Allen, J.O., Fergenson, D.P., Gard, E.E., Hughes, L.S., Morrical, B.D., Kleeman, M.J., Gross, D.S., Galli, M.E., Prather, K.A., Cass, G.R., 2000. Particle detection efficiencies of aerosol time of flight mass spectrometers under ambient sampling conditions. Environmental Science & Technology 34, 211–217.

Andreae, M.O., 1983. Soot carbon and excess fine potassium: long-range transport of combustion-derived aerosols. Science in China Series B – Chemistry 220, 1148–1151.

Andreae, M.O., Merlet, P., 2001. Emissions of trace gases and aerosols from biomass burning. Global Biogeochemistry Cycles 15, 955–966.

Angelino, S., Suess, D.T., Prather, K.A., 2001. Formation of aerosol particles from reactions of secondary and tertiary alkylamines: characterization by aerosol time-of-flight mass spectrometry. Environmental Science & Technology 35, 3130–3138.

Appel, B.R., Tokiwa, Y., Hsu, J., Kothny, E.L., Hahn, E., 1985. Visibility as related to atmospheric aerosol constituents. Atmospheric Environment 19, 1525–1534.

Bi, X.H., Simoneit, B.R.T., Sheng, G.Y., Ma, S.X., Fu, J.M., 2008. Composition and major sources of organic compounds in urban aerosols. Atmospheric Research 88, 256–265.

bin Abas, M.R., Oros, D.R., Simoneit, B.R.T., 2004. Biomass burning as the main source of organic aerosol particulate matter in Malaysia during haze episodes. Chemosphere 55, 1089–1095.

Bond, T., Habib, G., Bergstrom, R., 2006. Limitations in the enhancement of visible light absorption due to mixing state. Journal of Geophysical Research – Atmospheres 111, D20211. doi:10.1029/2006JD007315.

Cheng, Y.F., Wiedensohler, A., Eichler, H., Su, H., Gnauk, T., Brueggemann, E., Herrmann, H., Heintzenberg, J., Slanina, J., Tuch, T., Hu, M., Zhang, Y.H., 2008. Aerosol optical properties and related chemical apportionment at Xinken in Pearl River Delta of China. Atmospheric Environment 42, 6351–6372.

Dall'Osto, M., Beddows, D.C.S., Kinnersley, R.P., Harrison, R.M., Donovan, R.J., Heal, M.R., 2004. Characterization of individual airborne particles by using aerosol time-of-flight mass spectrometry at Mace Head, Ireland. Journal of Geophysical Research – Atmospheres 109. doi:10.1029/2004jd004747.

Dall'Osto, M., Harrison, R.M., 2006. Chemical characterisation of single airborne particles in Athens (Greece) by ATOFMS. Atmospheric Environment 40, 7614–7631.

Denkenberger, K.A., Moffet, R.C., Holecek, J.C., Rebotier, T.P., Prather, K.A., 2007. Real-time, single-particle measurements of oligomers in aged ambient aerosol particles. Environmental Science & Technology 41, 5439–5446.

Freney, E.J., Heal, M.R., Donovan, R.J., Mills, N.L., Donaldson, K., Newby, D.E., Fokkens, P.H.B., Cassee, F.R., 2006. A single-particle characterization of a mobile versatile aerosol concentration enrichment system for exposure studies. Part Fibre Toxicology 3, 8.

Gard, E., Mayer, J.E., Morrical, B.D., Dienes, T., Fergenson, D.P., Prather, K.A., 1997. Real-time analysis of individual atmospheric aerosol particles: design and performance of a portable ATOFMS. Analytical Chemistry 69, 4083–4091.

Gard, E.E., Kleeman, M.J., Gross, D.S., Hughes, L.S., Allen, J.O., Morrical, B.D., Fergenson, D.P., Dienes, T., Gälli, M.E., Johnson, R.J., Cass, G.R., Prather, K.A., 1998. Direct observation of heterogeneous chemistry in the atmosphere. Science 279, 1184–1187.

Gaston, C.J., Pratt, K.A., Qin, X.Y., Prather, K.A., 2010. Real-time detection and mixing state of methanesulfonate in single particles at an inland urban location during a phytoplankton bloom. Environmental Science & Technology 44, 1566–1572.

Guazzotti, S.A., Whiteaker, J.R., Suess, D., Coffee, K.R., Prather, K.A., 2001. Real-time measurements of the chemical composition of size-resolved particles during a Santa Ana wind episode, California USA. Atmospheric Environment 35, 3229–3240.

Gurciullo, C.S., Pandis, S.N., 1997. Effect of composition variations in cloud droplet populations on aqueous-phase chemistry. Journal of Geophysical Research – Atmospheres 102 (D8), 9375–9385.

Hagler, G.S., Bergin, M.H., Salmon, L.G., Yu, J.Z., Wan, E.C.H., Zheng, M., Zeng, L.M., Kiang, C.S., Zhang, Y.H., Lau, A.K.H., Schauer, J.J., 2006. Source areas and chemical composition of fine particulate matter in the Pearl River Delta region of China. Atmospheric Environment 40, 3802–3815.

Hu, M., Wu, Z.J., Slanina, J., Lin, P., Liu, S., Zeng, L.M., 2008. Acidic gases, ammonia and water-soluble ions in $PM_{2.5}$ at a coastal site in the Pearl River Delta, China. Atmospheric Environment 42, 6310–6320.

Hua, W., Chen, Z.M., Jie, C.Y., Kondo, Y., Hofzumahaus, A., Takegawa, N., Chang, C.C., Lu, K.D., Miyazaki, Y., Kita, K., Wang, H.L., Zhang, Y.H., Hu, M., 2008. Atmospheric hydrogen peroxide and organic hydroperoxides during PRIDE-PRD'06, China: their concentration, formation mechanism and contribution to secondary aerosols. Atmospheric Chemistry and Physics 8, 6755–6773.

Jacobson, M.Z., 2001. Strong radiative heating due to the mixing state of black carbon in atmospheric aerosols. Nature 409, 695–697.

Lee, S.H., Murphy, D.M., Thomson, D.S., Middlebrook, A.M., 2003. Nitrate and oxidized organic ions in single particle mass spectra during the 1999 Atalanta supersite project. Journal of Geophysical Research 108. doi:10.1029/2001JD001455.

Li, L., Huang, Z., Dong, J., Li, M., Gao, W., Nian, H., Fu, Z., Zhang, G., Bi, X., Cheng, P., Zhou, Z., 2011. Real time bipolar time-of-flight mass spectrometer for analyzing single aerosol particles. International Journal Mass Spectrometry. doi:10.1016/j.ijms.2011.01017.

Li, W.J., Shao, L.Y., 2009. Transmission electron microscopy study of aerosol particles from the brown hazes in northern China. Journal of Geophysical Research – Atmospheres 114. doi:10.1029/2008jd011285.

Li, W.J., Shao, L.Y., Buseck, P.R., 2010. Haze types in Beijing and the influence of agricultural biomass burning. Atmospheric Chemistry and Physics 10, 8119–8130.
Liu, D.Y., Wenzel, R.J., Prather, K.A., 2003. Aerosol time-of-flight mass spectrometry during the Atlanta Supersite Experiment: 1. Measurements. Journal of Geophysical Research – Atmospheres 108, 8426.
Moffet, R.C., Prather, K.A., 2009. In-situ measurements of the mixing state and optical properties of soot with implications for radiative forcing estimates. Proceedings of the National Academy of Sciences of the United States of America 106, 11872–11877.
Moffet, R.C., Shields, L.G., Bernsten, J., Devlin, R.B., Prather, K.A., 2004. Characterization of an ambient coarse particle concentrator used for human exposure studies: aerosol size distributions, chemical composition, and concentration enrichment. Aerosol Science and Technology 38, 1123–1137.
Murphy, D.M., Thomson, D.S., 1997. Chemical composition of single aerosol particles at Idaho Hill: positive ion measurements. Journal of Geophysical Research 102, 6341–6352.
Pastor, S.H., Allen, J.O., Hughes, L.S., Bhave, P., Cass, G.R., Prather, K.A., 2003. Ambient single particle analysis in Riverside, California by aerosol time-of-flight mass spectrometry during the SCOS97-NARSTO. Atmospheric Environment 37, S239–S258.
Pratt, K.A., Prather, K.A., 2009. Real-time, single-particle volatility, size, and chemical composition measurements of aged urban aerosols. Environmental Science & Technology 43, 8276–8282.
Pratt, K.A., Prather, K.A., 2010. Aircraft measurements of vertical profiles of aerosol mixing states. Journal of Geophysical Research – Atmospheres 115. doi:10.1029/2009jd013150.
Reid, J.S., Eck, T.F., Christopher, S.A., Koppmann, R., Dubovik, O., Eleuterio, D.P., Holben, B.N., Reid, E.A., Zhang, J., 2005a. A review of biomass burning emissions part III: intensive optical properties of biomass burning particles. Atmospheric Chemistry and Physics 5, 827–849.
Reid, J.S., Koppmann, R., Eck, T.F., Eleuterio, D.P., 2005b. A review of biomass burning emissions part II: intensive physical properties of biomass burning particles. Atmospheric Chemistry and Physics 5, 799–825.
Rose, D., Nowak, A., Achtert, P., Wiedensohler, A., Hu, M., Shao, M., Zhang, Y.H., Andreae, M.O., Poschl, U., 2010. Cloud condensation nuclei in polluted air and biomass burning smoke near the mega-city Guangzhou, China – part I: size-resolved measurements and implications for the modeling of aerosol particle hygroscopicity and CCN activity. Atmospheric Chemistry and Physics 10, 3365–3383.
Schmidl, C., Bauer, H., Dattler, A., Hitzenberger, R., Weissenboeck, G., Marr, I.L., Puxbaum, H., 2008. Chemical characterization of particle emissions from burning leaves. Atmospheric Environment 42, 9070–9079.
Shields, L.G., Qin, X.Y., Toner, S.M., Prather, K.A., 2008. Detection of ambient ultrafine aerosols by single particle techniques during the SOAR 2005 campaign. Aerosol Science and Technology 42, 674–684.
Silva, P.J., Liu, D.Y., Noble, C.A., Prather, K.A., 1999. Size and chemical characterization of individual particles resulting from biomass burning of local Southern California species. Environmental Science & Technology 33, 3068–3076.
Sodeman, D.A., Toner, S.M., Prather, K.A., 2005. Determination of single particle mass spectral signatures from light-duty vehicle emissions. Environmental Science & Technology 39, 4569–4580.
Spencer, M.T., Holecek, J.C., Corrigan, C.E., Ramanathan, V., Prather, K.A., 2008. Size-resolved chemical composition of aerosol particles during a monsoonal transition period over the Indian Ocean. Journal of Geophysical Research – Atmospheres 113, D16305. doi:10.1029/2007JD008657.
Spencer, M.T., Prather, K.A., 2006. Using ATOFMS to determine OC/EC mass fractions in particles. Aerosol Science and Technology 40, 585–594.
Streets, D.G., Gupta, S., Waldhoff, S.T., Wang, M.Q., Bond, T.C., Bo, Y.Y., 2001. Black carbon emissions in China. Atmospheric Environment 35, 4281–4296.
Su, Y.X., Sipin, M.F., Furutani, H., Prather, K.A., 2004. Development and characterization of an aerosol time-of-flight mass spectrometer with increased detection efficiency. Analytical Chemistry 76, 712–719.
Sugimoto, N., Nishizawa, T., Liu, X.G., Matsui, I., Shimizu, A., Zhang, Y.H., Kim, Y.J., Li, R.H., Liu, J., 2009. Continuous observations of aerosol profiles with a two-wavelength Mie-scattering lidar in Guangzhou in PRD2006. Journal of Applied Meteorology and Climatology 48, 1822–1830.
Toner, S.M., Sodeman, D.A., Prather, K.A., 2006. Single particle characterization of ultrafine and accumulation mode particles from heavy duty diesel vehicles using aerosol time-of-flight mass spectrometry. Environmental Science & Technology 40, 3912–3921.
Tyndall, G.S., Ravishankara, A.R., 1991. Atmospheric oxidation of reduced sulfur species. International Journal of Chemical Kinetics 23, 483–527.
Wang, Q.Q., Shao, M., Liu, Y., Williams, K., Paul, G., Li, X.H., Liu, Y., Lu, S.H., 2007. Impact of biomass burning on urban air quality estimated by organic tracers: Guangzhou and Beijing as cases. Atmospheric Environment 41, 8380–8390.
Wang, X.F., Zhang, Y.P., Chen, H., Yang, X., Chen, J.M., 2009a. Particulate nitrate formation in a highly polluted urban area: a case study by single-particle mass spectrometry in Shanghai. Environmental Science & Technology 43, 3061–3066.
Wang, Z.Z., Bi, X.H., Sheng, G.Y., Fu, J.M., 2009b. Characterization of organic compounds and molecular tracers from biomass burning smoke in South China I: broad-leaf trees and shrubs. Atmospheric Environment 43, 3096–3102.
Warneke, C., Bahreini, R., Brioude, J., Brock, C.A., de Gouw, J.A., Fahey, D.W., Froyd, K.D., Holloway, J.S., Middlebrook, A., Miller, L., Montzka, S., Murphy, D.M., Peischl, J., Ryerson, T.B., Schwarz, J.P., Spackman, J.R., Veres, P., 2009. Biomass burning in Siberia and Kazakhstan as an important source for haze over the Alaskan Arctic in April 2008. Geophysical Research Letters 36. doi:10.1029/2008gl036194.
Xiao, R., Takegawa, N., Kondo, Y., Miyazaki, Y., Miyakawa, T., Hu, M., Shao, M., Zeng, L.M., Hofzumahaus, A., Holland, F., Lu, K., Sugimoto, N., Zhao, Y., Zhang, Y.H., 2009. Formation of submicron sulfate and organic aerosols in the outflow from the urban region of the Pearl River Delta in China. Atmospheric Environment 43, 3754–3763.
Yamasoe, M.A., Artaxo, P., Miguel, A.H., Allen, A.G., 2000. Chemical composition of aerosol particles from direct emissions of vegetation fires in the Amazon Basin: water-soluble species and trace elements. Atmospheric Environment 34, 1641–1653.
Yang, F., 2010. Application of Single particle Time-of-flight Mass Spectrometry (ATOFMS) in the Study of Mixing State of Aerosols Research in Urban Atmosphere. Ph.D. Thesis. Fudan University.
Yang, F., Chen, H., Wang, X.N., Yang, X., Du, J.F., Chen, J.M., 2009. Single particle mass spectrometry of oxalic acid in ambient aerosols in Shanghai: mixing state and formation mechanism. Atmospheric Environment 43, 3876–3882.
Yu, H., Wu, C., Wu, D., Yu, J.Z., 2010. Size distributions of elemental carbon and its contribution to light extinction in urban and rural locations in the pearl river delta region, China. Atmospheric Chemistry and Physics 10, 5107–5119.
Zhang, Y.H., Hu, M., Zhong, L.J., Wiedensohler, A., Liu, S.C., Andreae, M.O., Wang, W., Fan, S.J., 2008. Regional integrated experiments on air quality over Pearl River delta 2004 (PRIDE-PRD2004): overview. Atmospheric Environment 42, 6157–6173.
Zhang, Y.P., Kreidenweis, S.M., Feingold, G., 1999. Stratocumulus processing of gases and cloud condensation nuclei 2. Chemistry sensitivity analysis. Journal of Geophysical Research – Atmospheres 104, 16061–16080.